Journal of ELECTRONIC MATERIALS, Vol. 46, No. 7, 2017
DOI: 10.1007/s11664-017-5451-7

Effects of Er^{3+} and Pr^{3+} Substitution on Structural, Dielectric, Ferroelectric and Photoluminescence Properties of the $BaTi_{0.9}Zr_{0.1}O_3$ Ceramic

I. ZOUARI,[1,3] Z. SASSI,[2] L. SEVEYRAT,[2] V. PERRIN,[2] S. ZGHAL,[1] N. ABDELMOULA,[1] L. LEBRUN,[2] and H. KHEMAKHEM[1]

1.—Laboratory of Multifunctional Materials and Applications (LaMMA), LR16ES18, Faculty of Sciences of Sfax, University of Sfax, BP 1171, 3000 Sfax, Tunisia. 2.—Univ Lyon, INSA-LYON, LGEF, EA682, 69621 Villeurbanne, France. 3.—e-mail: ilhemz.ilhem89@gmail.com

$BaTi_{0.9}Zr_{0.1}O_3$ (BZT), $Ba_{1-x}Ln_{2x/3}\square_{x/3}Ti_{0.9}Zr_{0.1}O_3$ (with x = 0.5% mol and Ln = Er) (BZT-Er) and $Ba_{1-x}Ln_{2x/3}\square_{x/3}Ti_{0.9}Zr_{0.1}O_3$ (with x = 0.5% mol and Ln = Pr) (BZT-Pr) were prepared via the conventional solid-state reaction method. X-ray diffraction showed that all these ceramics were in the single perovskite phase at room temperature (RT). The temperature dependence of dielectric behavior was investigated in the temperature range 25–225°C and exhibited a classical ferroelectric behavior. A slight decrease of the Curie temperature (T_C) with Pr^{3+} and Er^{3+} substitution was observed in addition to an increase in the maximum dielectric permittivity ($\varepsilon'_{r\,max}$) of about 40% for the BZT-Er. At RT, the ferroelectric and piezoelectric coefficients were decreased for BZT-Pr, but were maintained for BZT-Er with a piezoelectric coefficient (d_{33}) of 185 pC/N, a planar electromechanical coupling factor of 30%, and a remanent polarization of 11.6 $\mu C/cm^2$. The Raman bands as a function of temperature confirmed the paraelectric-ferroelectric phase transition of all those ceramics. The photoluminescence spectra showed that strong red (615 nm and 645 nm) and bright green (523 nm and 545 nm) emission bands were obtained, under excitation by laser at 488 nm at RT, for BZT-Pr and BZT-Er, respectively. These multifunctional materials showed a significant technological promise in coupling device applications.

Key words: Ceramics, dielectric, ferroelectric, piezoelectric, photoluminescence, multifunctional

INTRODUCTION

$BaTiO_3$-based solid solutions are environmentally-friendly materials with similar ferroelectric and piezoelectric performances compared to Pb-based ceramics.[1,2] The Barium zirconate titanate ($BaZr_xTi_{1-x}O_3$) system is one of the first $BaTiO_3$ -based solid solutions studied for potential applications such as piezoelectric transducers, dynamic random access memory (DRAM), tunable microwave devices, and electrical energy storage units.[3–6] The ferroelectric properties of these $Ba(Zr_xTi_{1-x})O_3$ materials are largely dependent on the amount of Zr substitution.[7] The substitution of Ti^{4+} by Zr^{4+} in the $BaTiO_3$ ceramic improves the dielectric behavior. Up to 20% mol of Zr, a classical ferroelectric behavior is obtained with a Curie temperature (T_C) above room temperature (RT) and a high dielectric constant.[7] For higher contents, a relaxor behavior is observed and the T_C falls below RT.[8] The $BaTi_{0.9}Zr_{0.1}O_3$ (BZT) ceramic is interesting due to its high dielectric constant, low dielectric loss and a T_C above RT.[8–10]

In addition, some studies have been done to improve the dielectric, piezoelectric, ferroelectric and photoluminescence (PL) properties of the $BaTiO_3$-based ferroelectric ceramics with low

(Received October 24, 2016; accepted March 13, 2017; published online March 31, 2017)

substitutions of rare earth ions.[11,12] The $BaZr_xTi_{1-x}O_3$ solid solutions have been doped with different lanthanides such as Samarium, Europium, Dysprosium and Ytterbium.[10,13] Praseodymium (Pr) and Erbium (Er) rare earth elements are significantly used to influence the luminescent and piezoelectric properties.[14–17]

Moreover, Zhao et al.[18] have shown that the addition of Er_2O_3 to the (K, Na)NbO_3 ceramics improves the piezoelectric and PL properties of such ceramics. The maximum value of the piezoelectric coefficient (d_{33}) has been obtained for ceramics with the addition of only 0.5% mol.[18] These materials have a low luminescent intensity or weak piezoelectric properties, which constrain their practical applications in integrated optical and electrical devices. As a consequence, several efforts have been made to obtain lead-free ferroelectric matrices and to improve their properties.

For this purpose, the $BaTi_{0.9}Zr_{0.1}O_3$ (BZT) composition has been chosen and the rare earth elements Pr^{3+} and Er^{3+} have been used to obtain a multifunctional material. In this work, the effects of the low content of rare earth (0.5% mol of Pr^{3+} and Er^{3+}) on the structural, dielectric, piezoelectric, ferroelectric and PL properties of these ceramics are investigated.

EXPERIMENTAL

Based on the A-site vacancy defect compensation model, ceramics are obtained using the formula $Ba_{1-x}Ln_{2/3x}\square_{x/3}Ti_{0.9}Zr_{0.1}O_3$, where $\square$ represents vacancies in the crystalline structure.[13,19–21] $BaTi_{0.9}Zr_{0.1}O_3$ (BZT), $Ba_{1-x}Ln_{2x/3}\square_{x/3}Ti_{0.9}Zr_{0.1}O_3$ (with x = 0.5% mol and Ln = Er) (BZT-Er) and $Ba_{1-x}Ln_{2x/3}\square_{x/3}Ti_{0.9}Zr_{0.1}O_3$ (with x = 0.5% mol and Ln = Pr) (BZT-Pr) compositions were prepared by the conventional solid-state reaction method.

The starting materials are highly pure powders of $BaCO_3$ (Aldrich 99%), ZrO_2 (Aldrich 99%), TiO_2 (Aldrich > 99%), Pr_6O_{11} (Aldrich 99.9%) and Er_2O_3 (Aldrich 99.9%). All these materials were dried at 150°C for 2 h, weighed, mixed and milled in an alcoholic medium for 1 h. The mixtures were calcined at 1250°C for 12 h in air. The obtained powders, to which a 5% mass of polyvinyl alcohol (PVA) was added, were mixed for 1 h and pressed under 100 MPa into 8 mm diameter and about 1 mm thick pellets. Finally, the pellets were heated at 600°C for 4 h in order to eliminate the organic products, and then were sintered at 1450°C for 4 h with a heating rate of 250°C/h. RT powder x-ray diffraction (XRD) patterns were recorded on a Philips diffractometer using CuKα_1 and CuKα_2 radiation (λ_1 = 1.540598 Å, λ_2 = 1.544426 Å) in the range $10° \le 2\theta \le 80°$ with a step of 0.02° in order to determine the structure of all the prepared ceramic compositions. Dielectric measurements were performed on the ceramic discs after deposition of silver electrodes on both sides. The dielectric permittivity of the sample was measured as a function of both temperature (25–225°C) and frequency (10^3–10^5 Hz). The d_{33} was measured using a YE2730A d_{33}-meter at RT. The electromechanical coupling factor (k_p) was calculated with the resonance-antiresonance method using the HP4194A impedance analyzer. Ferroelectric (P–E) loops were determined at RT by applying a maximum electric field of 3 kV/mm at a frequency of 1 Hz. The ceramic sample was immersed in a thermostatic oil bath. The current and the electric field were recorded while applying cyclic electric fields using a current amplifier (Keithley 428) and a high voltage amplifier (TREK Model 20/20C). The working frequency was fixed at 1 Hz. Raman scattering data were collected in the frequency range (50–850 cm^{-1}) using a Raman spectrometer (Horiba HR 800, Jobin–Yvon). PL measurements were performed on a Cornerston 260 monochromator (from Oriel instruments) coupled with an R955 photomultiplier (Hamamatsu, Japan). A multi-line Lasos Argon laser with an output power of 40 mW and a selected wavelength of 488 nm were used as the excitation source. PL spectra were repeated three times for each sample to ensure reliable results. All the measurements were performed at RT.

RESULTS AND DISCUSSION

X-ray Diffraction Study

Figure 1 exhibits the XRD patterns of BZT, BZT-Pr and BZT-Er specimens. The intensities of XRD patterns for these ceramics are plotted in Fig. 1a using a logarithmic axis. Two very low intensity peaks were observed around 2θ values of 28° and 34°; these are indicated by '*' in Fig. 1a. According to Byoung-Ki Lee et al.[22] they may be associated with the Ba-deficient phase $Ba_6Ti_{17}O_{40}$.[22,23] The Rietveld refined XRD patterns, which were indexed in rhombohedral structure (with R3m space group) using the Fullprof suite program,[24] of BZT, BZT-Pr and BZT-Er are shown in Fig. 1b, c, and d, respectively.

Table I indicates the lattice-parameter refinements for each synthesized compound. Since the ionic radii of Pr^{3+} (1.126 Å, 8 coordinate) and Er^{3+} (1.004 Å, 8 coordinate) are small compared to those of Ba^{2+} (1.42 Å, 8 coordinate),[25] then the increase in the unit cell volume is due to the strain developed within the crystal lattice, which in turn is due to the small mismatch between the ionic radii of the Ba^{2+} ions and those of the Pr^{3+} and Er^{3+} ions.[19,26]

Raman Spectroscopy Characterization

Depolarized Raman spectra of all the BZT and BZT-Ln (BZT-Pr and BZT-Er) compositions at RT, using the 633 nm line of an Ar ion laser for BZT and BZT-Pr and using the 488 nm for BZT and BZT-Er, are presented in Fig. 2. It can be noted that the Raman measurement using 633 nm seems to be

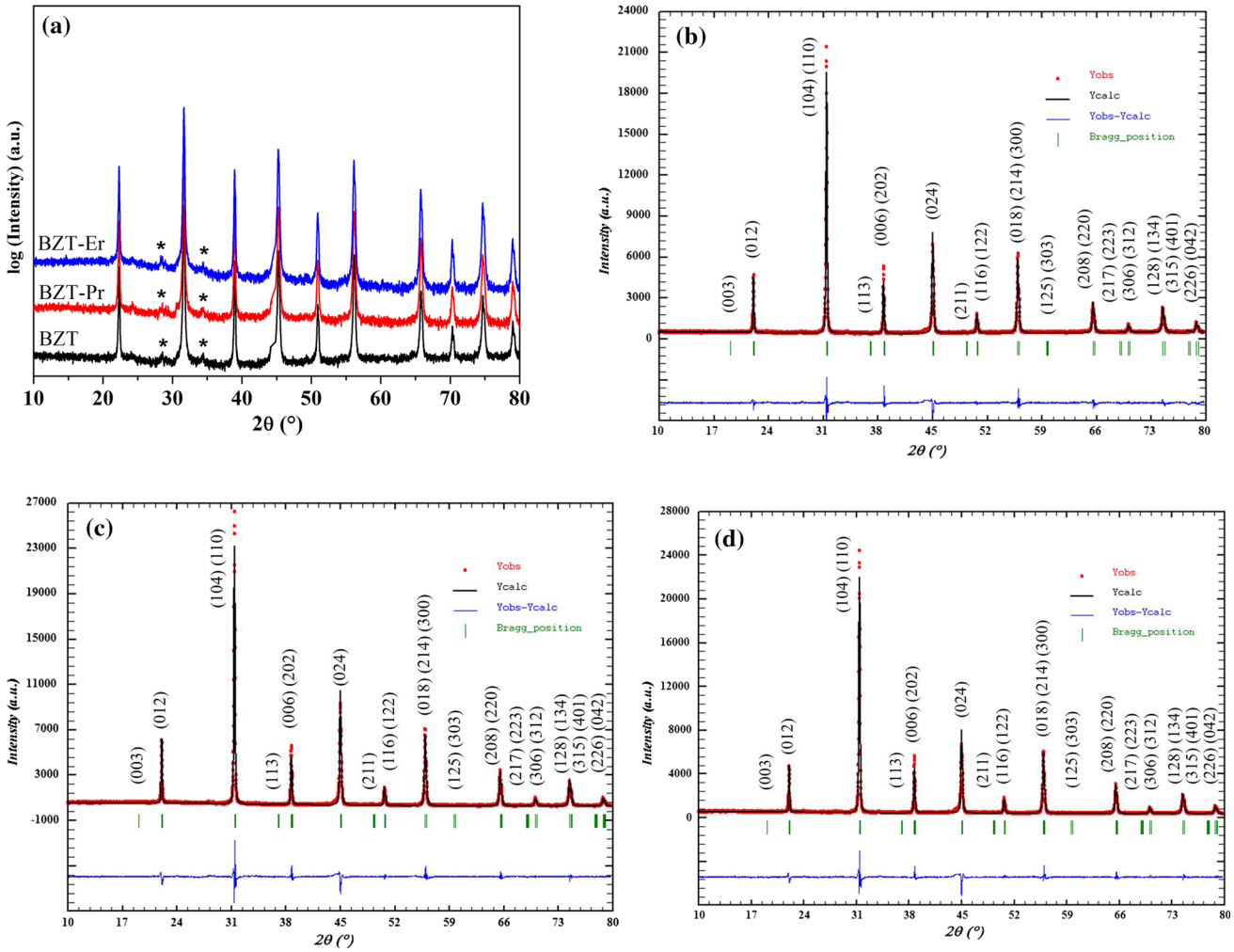

Fig. 1. Room temperature XRD patterns of BZT and BZT-Ln compounds: (a) Logarithmic intensities of XRD patterns for each ceramic, (b), (c) and (d) Rietveld refined XRD patterns of BZT, BZT-Er and BZT-Pr, respectively.

Table I. Crystallographic data of BZT and BZT-Ln compounds obtained by the solid-state reaction

	Rhombohedral structure (R3m)		
Parameters	**BZT**	**BZT-Pr**	**BZT-Er**
a (Å)	5.693 (4)	5.693 (6)	5.693 (4)
c (Å)	13.947 (2)	13.958 (8)	13.958 (3)
V (Å^3)	391.526 (4)	391.879 (5)	391.838 (0)

very sensitive to the introduction of the Er^{3+} with an optical activity, where interesting changes in the local symmetry could be revealed. In order to eliminate this luminescence effect, a 488 nm light excitation for BZT-Er was used. The same effect was observed by other authors in the literature.[27]

The attribution of the bands was done from bibliographical data.[28,29] So, the Raman spectrum of the BZT and BZT-Ln showed the commonly reported $E(TO_1)$, $A_1(TO_1)$, $A_1(LO)$, $A_1(TO_2)$, B_1 + E(TO + LO), $A_1(LO_2)$ + E(LO), $A_1(TO_3)$ + E(TO), $A_1(LO_3)$ + E(LO) and A_{1g} optical modes, peaking at approximately 110 cm^{-1}, 167 cm^{-1}, 197 cm^{-1}, 257 cm^{-1}, 302 cm^{-1}, 475 cm^{-1}, 520 cm^{-1}, 720 cm^{-1}, and 800 cm^{-1}, respectively.

Moreover, compared to those of BZT, all the bands of BZT-Pr and BZT-Er show a slight broadening, a weaker intensity and a slight shift to higher frequencies. This could be connected to the disorder created by the substitution of Ba^{2+} by Ln^{3+} in the BZT ceramic.

The thermal evolution of the Raman spectrum of the ceramic compositions BZT, BZT-Pr and BZT-Er

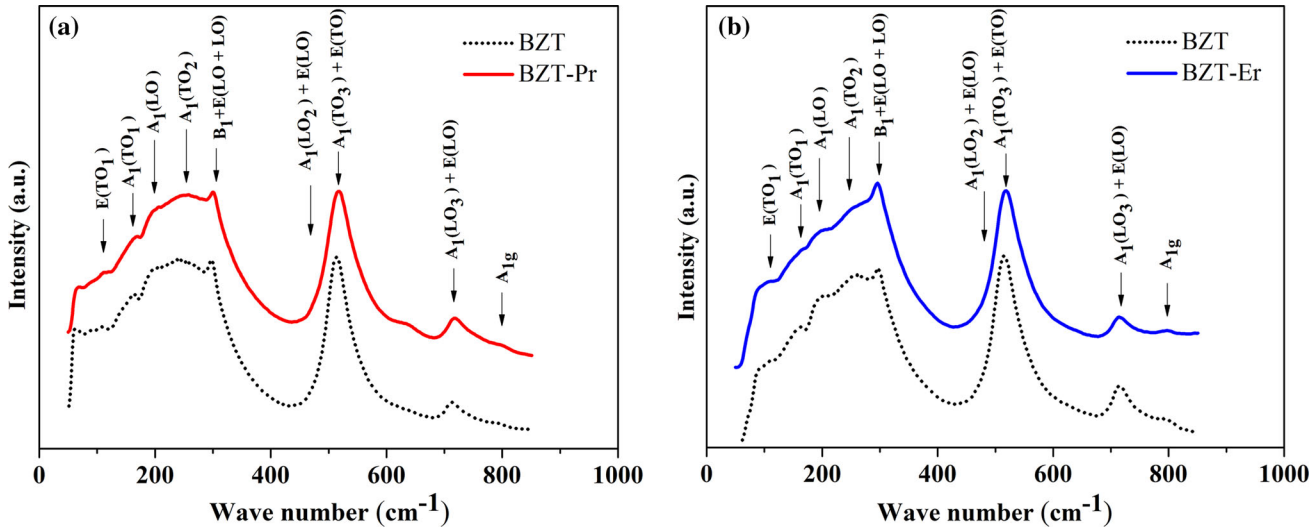

Fig. 2. Raman spectra of various BZT and BZT-Ln compounds at room temperature: (a) using laser with a 633 nm excitation for each BZT and BZT-Pr, (b) using laser with a 488 nm excitation for each for BZT and BZT-Er.

for the wide frequency range (50–850 cm^{-1}) and the position of the observed modes are shown in Fig. 3a, b, and c, respectively. With an increase in temperature, a broadening of all the Raman bands and a remarkable decrease in intensity are observed as the temperature increases, especially after T_C = 88°C, 80°C, and 84°C in BZT, BZT-Pr and BZT-Er, respectively. This behaviour characterizes the important disorder introduced at high temperature.[30,31] After T_C, all modes disappear from the paraelectric phase, but some broad bands persist. The origin of their activation in the para-electric phase should be found in a local short range polar order.

Dielectric Properties

The temperature dependences of the real parts of the permittivity (ε'_r) and losses ($\tan\delta$) for BZT, BZT-Er and BZT-Pr ceramics are given in Fig. 4a, b, and c, respectively.

For BZT, in the plot of permittivity as a function of temperature, three anomalies are observed related to the rhombohedral-to-orthorhombic, orthorhombic-to-tetragonal and tetragonal-to-cubic phase transitions, close to the temperature range (64–88°C) and with no significant frequency dispersion. For BZT-Er, the transition temperatures decrease. They are observed in the temperature range (58–84°C) always without frequency dispersion. The peak at the T_C is relatively sharp. The dielectric properties of this compound are greatly improved; indeed the maximum dielectric permittivity ($\varepsilon'_{r\,max}$) increases from 7476 for BZT to 11,683 for BZT-Er. However, in BZT-Pr, the three anomalies pinch in one broad transition. This result can be explained by the fact that the largest substituted ionic radii Pr^{3+} will result in more disorder of ferroelectric domains. The value of $\varepsilon'_{r\,max}$ of BZT-Pr was slightly higher than that of BZT; at T_C, the $\varepsilon'_{r\,max}$ of BZT-Pr was 8269. Moreover, for this composition, there was a small frequency dispersion of the dielectric permittivity, but the value of T_C was not dependent on frequency. It is remarkable that the BZT-Pr ceramic has the highest dielectric constant at RT compared to the BZT and BZT-Er ceramics. In fact, the relative dielectric permittivity ε'_r characterizes the interaction between the electric dipoles under electrical stress (for example, the application of a weak alternating electric field). As already noted, the ionic radius of Pr^{3+} is larger than that of Er^{3+}. As a consequence, and considering that the unit cell volume remains almost invariant, the distortion of the lattice structure of the BZT ceramic is greatly intensified when Ba^{2+} is substituted by Pr^{3+}, which promotes an increase in the space allowed for the movement of Ti^{4+} and then an increase of the interaction between the electric dipoles.[32]

The lower decrease in the T_C of BZT-Pr and BZT-Er compared to that of pure BZT could be explained by the following Eq. 1:

$$T_C = (K_L - K_S)/B, \quad (1)$$

where K_L is the long-range electrostatic force constant, K_S is the short-range harmonic restoring force constant, and B is the anharmonic coefficient.[10,33,34] The distortion of the lattice structure, due to the substitution of Ba^{2+} by Ln^{3+} ions, causes an increase in the short range harmonic restoring force in Ln-doped BZT ceramics and then causes a decrease of T_C. Furthermore, as already noted, the distortion in BZT-Pr is greater than that in BZT-Er. This fact leads to a decreased value of T_C in the BZT-Pr ceramic.[32] A similar result was obtained by Chou et al.[10] for other compositions and other rare-earths.

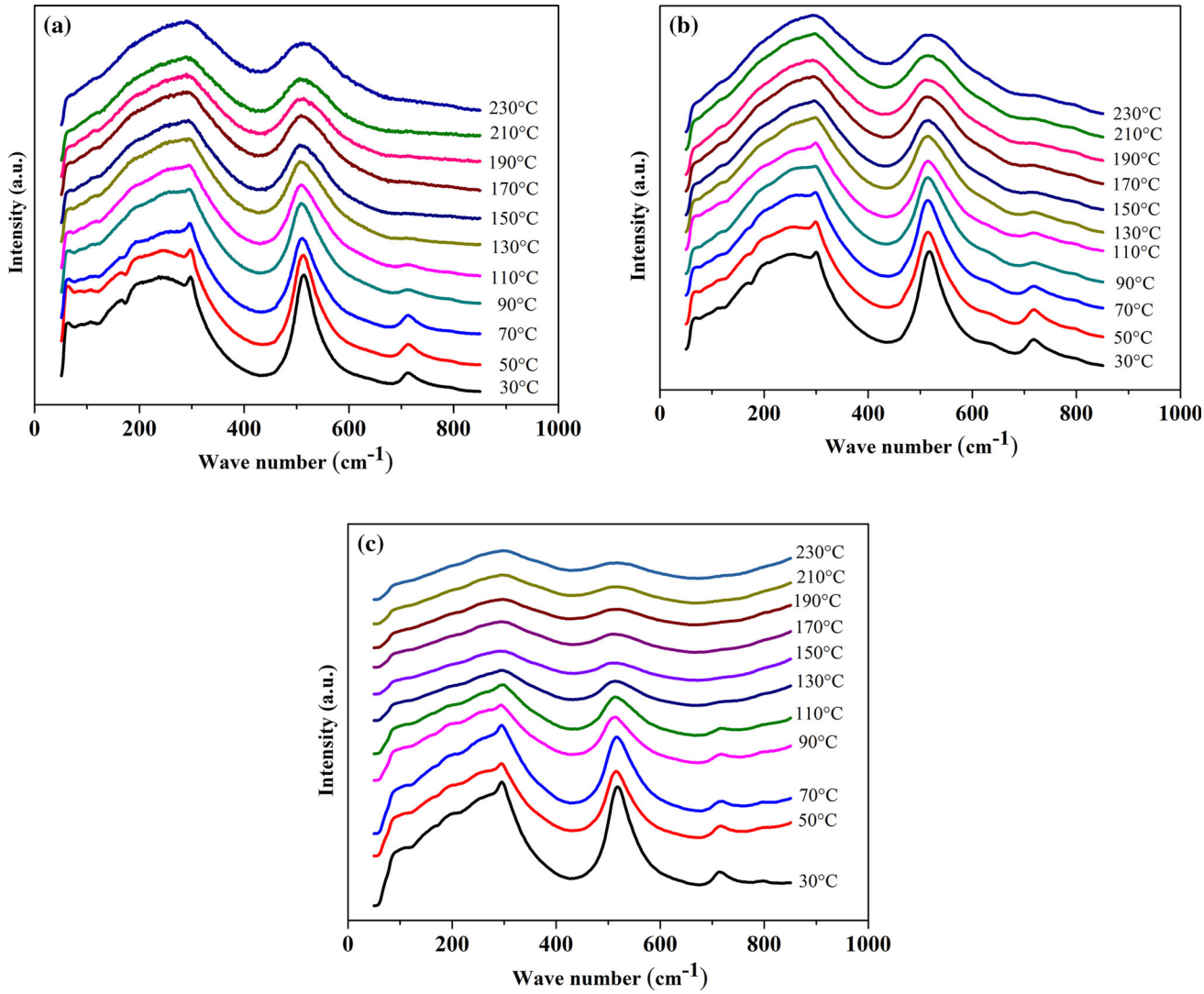

Fig. 3. Temperature dependence of the Raman spectra of BZT (a), BZT-Pr (b) and BZT-Er (c) over the wave number range 50–850 cm^{-1}.

Moreover, the dielectric loss ($\tan\delta$) for three selected frequencies (10^3 Hz, 10^4 Hz, and 10^5 Hz) is in the range of 0.09–0.28, 0.14–0.23 and 0.05–0.15 near T_C for BZT, BZT-Er and BZT-Pr respectively. Due to the phase transition, the dielectric loss reaches a maximum value and then decreases up to RT. At 25°C, it is in the range of 0.04–0.08, 0.07–0.08 and 0.05–0.09 for BZT, BZT-Er and BZT-Pr, respectively. This result reveals a good dielectric property in all compositions due to the fact that the dielectric losses are relatively low in the ferroelectric phase ($T < T_C$).

In addition, in BZT and BZT-Ln, the temperature variation of $(1/\varepsilon'_r)$ at 10 kHz is in agreement with a Curie–Weiss law for $T > T_C$ (see inset Fig. 4). The phase transition of all the ceramics, based on the theory of Landau, is of first order type ($T_C \neq T_0$), where T_0 is the Curie–Weiss temperature.[35]

On the other hand, the classical ferroelectric behaviour of the BZT ceramic is conserved by the substitution of Ba^{2+} by Ln^{3+}. In fact, the T_C and the associated maximum are independent of frequency.

Ferroelectric and Piezoelectric Properties

The hysteresis loops of polarization versus the electric field of the BZT and BZT-Ln ceramics measured at RT and at a frequency of 1 Hz are shown in Fig. 5. A high electric field (3 kV/mm) was required to obtain the saturation of the polarization.

The remanent polarization (P_r) and the coercive field (E_c) determined from the hysteresis loop for the BZT, BZT-Pr and BZT-Er ceramics are presented in Table II, with the values of d_{33} piezoelectric coefficient, k_p planar coupling factor, T_C, $\varepsilon'_{r\,max}$ at T_C and ε'_r at RT. Pure BZT shows a well-saturated P–E hysteresis loop with similar polarization values to those reported in the literature.[36] It is remarkable that when Ba^{2+} was substituted by Pr^{3+} in the BZT ceramic, the value of P_r decreased, but the value of E_c remained unchanged. However, when Ba^{2+} was

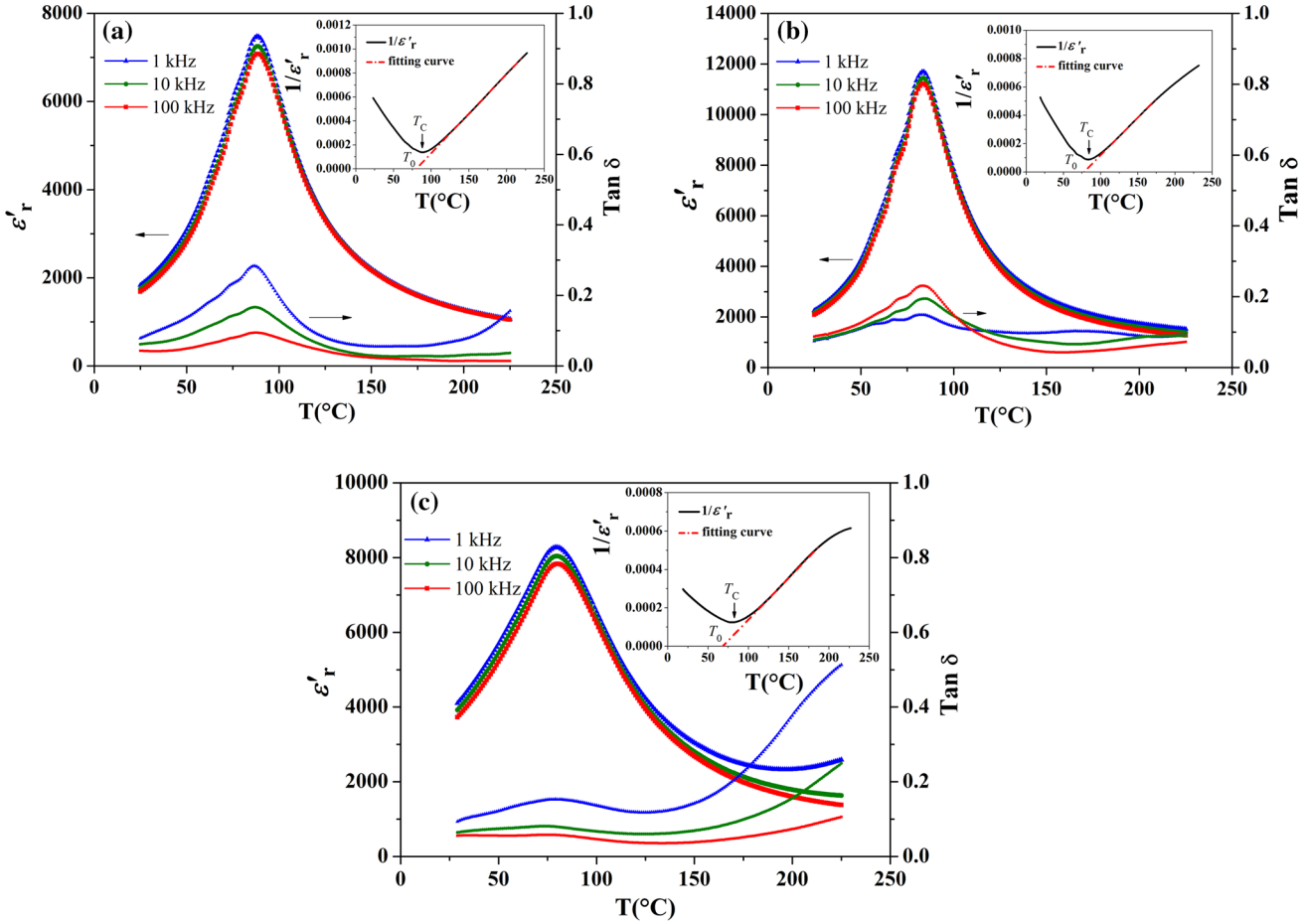

Fig. 4. Temperature dependence of the real parts of the permittivity and dielectric loss of BZT and BZT-Ln ceramics at frequencies from 1 kHz to 100 kHz: (a) BZT; (b) BZT-Er and (c) BZT-Pr. The right inset is the inverse of the dielectric constant ($1/\varepsilon'_r$) as a function of temperature at 10 kHz.

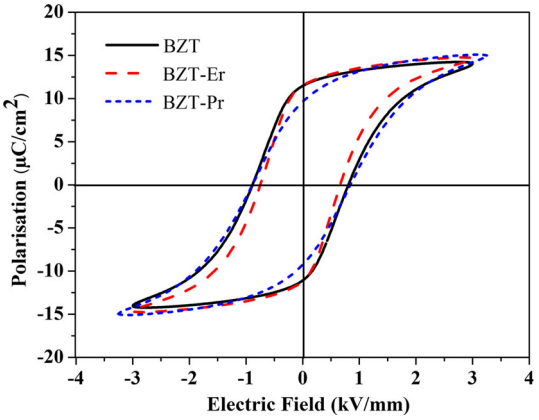

Fig. 5. Room temperature *P-E* hysteresis loop of BZT and BZT-Ln at 1 Hz.

substituted by Er^{3+} in the BZT ceramic, the value of P_r remained unchanged and the value of E_c decreased slightly. Based on the literature,[21] the decrease in the value of P_r and E_c is due to A-site vacancies. Assembling these vacancies at the domain boundary causes domain pinning which decreases P_r and E_c.[21] As already noted, BZT-Pr and BZT-Er prepared ceramics are of the A-site deficient perovskite type. This explains the decrease of P_r in BZT-Pr and E_c in BZT-Er. As already observed in dielectric measurements, the disorder ferroelectric domains in BZT-Pr are greater than those in BZT-Er. This explains the decrease of P_r and the increase of E_c in BZT-Pr compared to BZT-Er.

On the other hand, P_r and d_{33} have similar variations in the BZT and BZT-Ln ceramics. This proportionality between P_r and d_{33} is explained through the thermodynamic theory of ferroelectrics by the following Eq. 2[37]:

$$d_{33} = 2Q_{11} \cdot P_r \cdot \varepsilon_{33}, \qquad (2)$$

where Q_{11} is a constant representing the electrostrictive coefficient and ε_{33} is the dielectric constant. The values of d_{33} and k_p are 185, 90, 185 and 29.9%, 29.7%, 29.9% respectively for BZT, BZT-Pr, BZT-Er. Moreover, it is noticed that the value of the piezoelectric coefficient (d_{33} = 185 pC N^{-1}) for the composition BZT-Er can be considered as important compared to some values obtained in other ceramics like the 0.5% Er_2O_3 doped (K, Na)NbO_3 ceramic (d_{33} = 132 pC N^{-1}).[18]

Table II. Values of P_r, E_c, d_{33}, k_p, T_C and $\varepsilon'_{r\,max}$ parameters measured at T_C and the value of ε'_r measured at room temperature for BZT and BZT-Ln compounds

	P_r (μC/cm^2)	E_c (kV/mm)	d_{33} (pC/N)	k_p (%)	T_C (°C)	$\varepsilon'_{r\,max}$ at T_C	ε'_r at RT
BZT	11.6	0.79	185	29.9	88	7476	1832
BZT-Pr	9.5	0.79	90	29.7	80	8269	3867
BZT-Er	11.6	0.65	185	29.7	84	11683	2254

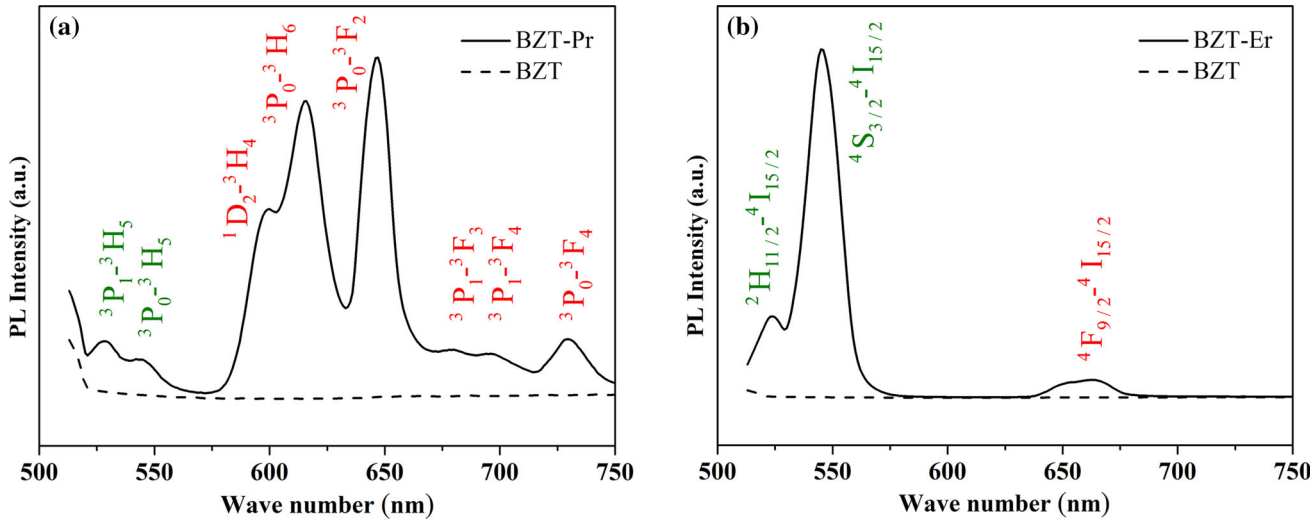

Fig. 6. PL spectra of BZT and BZT-Ln: (a) BZT-Pr with BZT and (b) BZT-Er with BZT.

Photoluminescence Properties

Upon a 488 nm laser excitation, it is noticed that BZT-Pr and BZT-Er exhibit luminescent properties which do not exist in the target ceramic BZT.

In Fig. 6a, for the BZT-Pr ceramic, the PL spectra consist of green and red emissions from the 520 nm to 750 nm regions wherein the green light of Pr^{3+} shows two emission peaks in the visible region centered at 527 nm and 545 nm, whereas the red emission shows six emission peaks located at 600 nm, 615 nm, 645 nm, 677 nm, 695 nm, and 730 nm, respectively. The 488 nm photon absorption causes excitation to the $^3P_0$ level of Pr^{3+}.[38] The green and red emission peaks are attributed to the ($^3P_1 \rightarrow {}^3H_5$), ($^3P_0 \rightarrow {}^3H_5$), ($^1D_2 \rightarrow {}^3H_4$), ($^3P_0 \rightarrow {}^3H_6$), ($^3P_0 \rightarrow {}^3F_2$), ($^3P_1 \rightarrow {}^3F_3$), ($^3P_1 \rightarrow {}^3F_4$) and ($^3P_0 \rightarrow {}^3F_4$) transitions respectively.[11]

The PL spectra of the BZT-Er sample under a 488 nm laser excitation at RT are shown in Fig. 6b. The strong green emission peaks near 523 nm and 545 nm are attributed to the $^2H_{11/2} \rightarrow {}^4I_{15/2}$ and $^4S_{3/2} \rightarrow {}^4I_{15/2}$ transitions, respectively, and the weak red emission located at 660 nm is caused by the $^4F_{9/2} \rightarrow {}^4I_{15/2}$ transition.[15] The mechanism of emission of materials containing Er^{3+} has been well-established in the literature.[15,39] When electrons are excited to the $^4F_{7/2}$ level upon a 488 nm light excitation, they non-radiatively relax to the $^2H_{11/2}$ and $^4S_{3/2}$ levels. From these levels, most of the excited Er^{3+} ions recombine to the ground state, producing green emissions at 523 nm and 545 nm. However, some of them relax to the $^4F_{9/2}$ level, leading to a weak red emission at 660 nm.

CONCLUSION

In this study, BZT and BZT-Ln materials were prepared by the conventional solid state method. The structural, dielectric, Raman, piezoelectric, ferroelectric and PL properties were investigated. It has been shown by XRD at RT that the structure of the compounds is rhombohedral. The dielectric measurements show a decrease of T_C and an improvement of the permittivity due to the substitution of Ba^{2+} by Ln^{3+} in the BZT ceramic. The good piezoelectric and ferroelectric properties of BZT are maintained in the BZT-Er composition. The substitution of Ba^{2+} by Pr^{3+} in BZT slightly decreases the remanent polarization (P_r) and piezoelectric coefficients at RT. Strong red (615 nm and 645 nm) emission bands are obtained for BZT-Pr and strong green (523 nm and 545 nm) emission bands are obtained for BZT-Er under excitation of a laser at 488 nm at RT, corresponding to the transitions $^3P_0 \rightarrow {}^3H_6$, $^3P_0 \rightarrow {}^3F_2$ for BZT-Pr and $^2H_{11/2} \rightarrow {}^4I_{15/2}$, $^4S_{3/2} \rightarrow {}^4I_{15/2}$ for BZT-Er, respectively. These results indicate that the BZT-Pr and BZT-Er materials can be used for integrated electro-optical devices as multifunctional materials. Our

work may provide a very effective mechanism of designing lead-free piezoelectric materials, luminescent materials and/or optical–electrical–mechanical couplings.

REFERENCES

1. F. Benabdallah, A. Simon, H. Khemakhem, C. Elissalde, and M. Maglione, *J. Appl. Phys.* 109, 124116 (2011).
2. J. Ravez and A. Simon, *Eur. Phys. J. Appl. Phys.* 11, 9 (2000).
3. Y. Zhi, A. Chen, R. Guo, and A.S. Bhalla, *J. Appl. Phys.* 92, 1489 (2002).
4. C.M. Wu, T.B. Wu, and M.L. Chen, *Appl. Phys. Lett.* 69, 2659 (1996).
5. X.G. Tang, J. Wang, X.X. Wang, and H.L.W. Chan, *Solid State Commun.* 131, 163 (2004).
6. J. Qi, Z. Gui, Y. Wang, Q. Li, T. Li, and L. Li, *J. Mater. Sci. Lett.* 21, 405 (2002).
7. H. Chen, C. Yang, C. Fu, J. Shi, J. Zhang, and W. Leng, *J. Mater. Sci.: Mater. Electron.* 19, 379 (2008).
8. S.B. Reddy, K. Prasad Rao, and M.S. Ramachandra Rao, *Scripta Mater.* 57, 591 (2007).
9. S.J. Kuang, X.G. Tang, L.Y. Li, Y.P. Jiang, and Q.X. Liu, *Scripta Mater.* 6, 68 (2009).
10. X. Chou, J. Zhai, H. Jiang, and X. Yao, *J. Appl. Phys.* 102, 084106 (2007).
11. Q. Zhang, H. Sun, X. Wang, Y. Zhang, and X. Li, *J. Eur. Ceram. Soc.* 34, 1439 (2014).
12. W. Li, Z. Xu, R. Chu, P. Fu, and G. Zang, *J. Alloys Compd.* 583, 305 (2014).
13. A. Kerfah, K. Taibi, A. Guehria-Laidoudi, A. Simon, and J. Ravez, *Solid State Sci.* 8, 613 (2006).
14. L. Guo, C. Zhong, X. Wang, and L. Li, *J. Alloys Compd.* 530, 22 (2012).
15. P. Du, L. Luo, W. Li, Y. Zhang, and H. Chen, *Mater. Sci. Eng., B* 178, 1219 (2013).
16. P. Du, L. Luo, W. Li, Y. Zhang, and H. Chen, *J. Alloys Compd.* 551, 219 (2013)..
17. P. Du, L. Luo, W. Li, Y. Zhang, and H. Chen, *J. Alloys Compd.* 559, 92 (2013).
18. Y. Zhao, X. Yuan, Y. Zhao, H. Zhou, J. Li, and HB. Jin, *Mater. Lett.* 162, 226 (2016).
19. C. Ostos, L. Mestres, M.L. Martinez-Sarrion, J.E. Garcia, A. Albareda, and R. Perez, *Solid State Sci.* 11, 1016 (2009).
20. J. Quan Qi, B. Bo Liu, H. Yong Tian, H. Zou, Z. Xing Yue, and L. Tu Li, *Solid State Sci.* 14, 1520 (2012).
21. M. Ganguly, S.K. Rout, T.P. Sinha, S.K. Sharma, H.Y. Park, C.W. Ahn, and I.W. Kim, *J. Alloys Compd.* 579, 473 (2013).
22. B.K. Lee, S.Y. Chung, and S.J.L. Kang, *J. Am. Ceram. Soc.* 83, 2858 (2000).
23. Y. Kaneko, F. Azough, T. Kida, K. Ito, T. Shimada, T. Minemura, B. Schaffer, and R. Freer, *J. Am. Ceram. Soc.* 95, 3928 (2012).
24. J. Rodriguez-Carvajal, Program Fullprof, Laboratoire Léon Brillouin, (CEA-CNRS), Version May 2009, LLB-JRC, (2010).
25. R.D. Shannon, *Acta Crystallogr. A* 32, 751 (1976).
26. S. Mahboob, A.B. Dutta, C. Prakash, G. Swaminathan, S.V. Suryanarayana, G. Prasad, and G.S. Kumar, *Mater. Sci. Eng., B* 134, 36 (2006).
27. M. Zannen, M. Dietze, H. Khemakhem, A. Kabadou, and M. ES-Souni, *Ceram. Int. B* 40, 13461 (2014).
28. V.S. Puli, D.K. Pradhan, W. Pérez, and R.S. Katiyar, *J. Phys. Chem. Solids* 74, 466 (2013).
29. J.C. Sczancoski, L.S. Cavalcante, T. Badapanda, S.K. Rout, S. Panigrahi, V.R. Mastelaro, J.A. Varela, M. Siu Li, and E. Longo, *Solid State Sci.* 12, 1160 (2010).
30. Y.J. Jiang, L.Z. Zeng, R.P. Wang, Y. Zhu, and L. Lia, *J. Raman Spectrosc.* 27, 31 (1996).
31. B. Wang and L. Zhang, *Phys. Status Solidi A* 169, 57 (1998).
32. Y. Zhi, A. Chen, P. M. Vilarinho, P. Q. Mantas, and J. L. Baptista, *J. Eur. Ceram. Soc.* 18, 1613 (1998).
33. X. Diez-Betriu, J.E. Garcia, C. Ostos, A.U. Boya, D.A. Ochoa, L. Mestres, and R. Perez, *Mater. Chem. Phys.* 125, 493 (2011).
34. Y. Chen, X. Dong, R. Liang, J. Li, and Y. Wang, *J. Appl. Phys.* 98, 064107 (2005).
35. D. Hennings, A. Schnell, and G. Simon, *J. Am. Ceram. Soc.* 65, 539 (1982).
36. F. Moura, A.Z. Simoes, B.D. Stojanovic, M.A. Zaghete, E. Longo, and J.A. Varela, *J. Alloys Compd.* 462, 129 (2008).
37. M.J. Haun, E. Furman, Z.Q. Zhuang, S.J. Jang, and L.E. Cross, *Ferroelectrics* 14, 313 (1989).
38. S.Q. Man, H.L. Zhang, Y.L. Liu, J.X. Meng, E.Y.B. Pun, and P.S. Chung, *Opt. Mater.* 30, 334 (2007).
39. S. Kuo, C. Chen, T. Tseng, S. Chang, and W. Hsieh, *J. Appl. Phys.* 92, 1868 (2002).